

The role of antibody-mediated immunity in shaping the seasonality of respiratory viruses

Ruarai Tobin^{a, b, †}, James McCaw^{a, b}, and Freya Shearer^{a, †}

^aSchool of Mathematics and Statistics, The University of Melbourne, Parkville 3010, Australia

^bInfectious Disease Dynamics Unit, Melbourne School of Population and Global Health, The University of Melbourne, Parkville 3010, Australia

[†]Corresponding authors: Ruarai J Tobin (ruarai.tobin@unimelb.edu.au) and Freya M Shearer (freya.shearer@unimelb.edu.au)

Abstract

In temperate regions, respiratory virus epidemics recur on a yearly basis, primarily during the winter season. This is believed to be induced by seasonal forcing, where the rate at which the virus can be transmitted varies cyclically across the course of each year. Seasonal epidemics can place substantial burden upon the healthcare system, with large numbers of infections and hospitalisations occurring across a short time period. However, the interactions between seasonal forcing and the factors necessary for epidemic resurgence — such as waning immunity, antigenic variation or demography — remain poorly understood. In this manuscript, we examine how the dynamics of antibody waning and antigenic variation can shape the seasonal recurrence of epidemics. We develop a susceptible-infectious-susceptible (*SIS*) immuno-epidemiological model of respiratory virus spread, where the susceptible population is stratified by their antibody level against the currently circulating strain of the virus, with this decaying as both antibody waning and antigenic drift occur. In the absence of seasonal forcing, we demonstrate the existence of two Hopf bifurcations over the effective antibody decay rate, with associated periodic model solutions. When seasonal forcing is introduced, we identify complex interactions between the strength of forcing and the effective antibody decay rate, yielding myriad dynamics including multi-year periodicity, quasiperiodicity and chaos. The timing and magnitude of seasonal epidemics is highly sensitive to this interaction, with the distribution of infection timing (by time of year) varying substantially across the parameter space. Finally, we show that seasonal forcing can produce resonant amplification (or damping) resulting in a cumulative infection burdens that is greater (or lesser) than would otherwise be observed.

1 Introduction

Respiratory viruses are a major cause of disease and mortality in human populations. It was estimated that in 2019, influenza led to between 290,000 and 640,000 deaths globally (Iuliano et al. 2018) and in the same year, respiratory syncytial virus (RSV) led to between 84,000 and 125,000 deaths globally in children aged under five years alone (Li et al. 2022). Further, the COVID-19 pandemic has highlighted the risks that a newly emergent respiratory virus can pose, with the disease having caused at least five million deaths by the end of 2021 (Msemburi et al. 2023).

A defining characteristic of the transmission of respiratory viruses is that they often produce recurring epidemics (or waves) of infection and disease across human populations. In temperate regions, this recurrence can be highly regular — for example, epidemics of the influenza viruses and respiratory syncytial virus are observed to occur every winter in temperate regions, with only rare exceptions (Altizer et al. 2006; Moriyama et al. 2020). This is believed to arise as a result of seasonal forcing, where the rate at which a virus may be transmitted changes cyclically across the course of each year, typically increasing in winter and decreasing in summer. Such changes could be driven by seasonal conditions directly (e.g. changing temperature, humidity or ultraviolet radiation leading to changes in virus stability across the transmission process, Moriyama et al. 2020; Nelson 2004) or indirectly (e.g. more close contact

occurring indoors during colder periods, London and Yorke 1973; Moriyama et al. 2020; Susswein et al. 2023).

The arisal of a sustained epidemic wave of infection is only possible where a sufficient proportion of the population is susceptible to infection with the pathogen. Recovery from infection with a respiratory virus typically leads to the development of adaptive immunity, which protects individuals from re-infection with the same virus and results in a depletion of the susceptible population. As such, the continued recurrence of epidemic waves implies the existence of one or more mechanisms which may replenish the susceptible population (Matt J Keeling and Rohani 2008). A number of such mechanisms have been suggested for respiratory viruses, including: demographic processes (with the introduction of new susceptible individuals via births or migration); waning immunity (where the immunity developed following infection is lost over time); and antigenic variation (where the virus evolves to evade the immunity present in individuals previously infected). In this work, we focus on the role that waning immunity and antigenic variation may play in providing the conditions for epidemic recurrence.

The antibody response is a key component of human immunity to respiratory virus infection. This response involves the production of large numbers of antibodies, proteins that can inhibit or neutralise the pathogen's ability to replicate within the host (Murphy and Weaver 2019). For some respiratory viruses, high levels of pathogen-specific antibodies produced following infection have been associated with a reduced probability of an individual developing infection following exposure to the virus. For example, studies of influenza and SARS-CoV-2 have identified dose-dependent relationships between antibody levels and protection from (symptomatic) infection (Hobson et al. 1972; Coudeville et al. 2010; Khoury et al. 2021; Phillips et al. 2024). However, if the quantity of these antibodies were to decay (or that of the B cells which produce them), this immune protection would be temporary (Andraud et al. 2012; Khoury et al. 2021).

In addition to antibody decay, the effectiveness of an individual's antibody response may decay with time due to antigenic variation. Where this occurs, an individual's effective antibody level against the currently circulating virus (as measured via e.g. viral neutralisation assays) will be reduced (R. G. Webster 1999; Medina and García-Sastre 2011). Such antigenic variation may occur as antigenic shift, where large changes in the antigen of the virus lead to sudden drops in the effectiveness of pre-existing antibodies, or as antigenic drift, where gradual changes in the virus accumulate and pre-existing antibodies become correspondingly less effective (R. Webster 1999; Kim et al. 2018). Such gradual antigenic drift is typical of many respiratory viruses, especially the influenza viruses (R. Webster 1999; Bedford, Suchard, et al. 2014).

In this paper, we construct an immuno-epidemiological model of respiratory virus transmission to study the interaction between antibody-mediated immunity and seasonal forcing. We begin in Section 2 by developing a susceptible-infectious-susceptible (*SIS*) model of virus transmission, where the susceptible population is stratified by antibody level. This antibody level increases upon recovery from infection, decays exponentially over time due to the combined effects of antibody waning and antigenic drift, and modulates an individual's protection against re-infection. In Section 3, we show that this model can exhibit periodicity in the absence of seasonal forcing and identify two Hopf bifurcations across the antibody decay rate. In Section 4, we introduce seasonal forcing into the model and examine its effect upon epidemiological dynamics. Our results show that forcing may interact with antibody-mediated immunity to produce complex dynamical regimes including quasiperiodicity and chaos, and identify that this interaction can lead to substantial changes in the distribution of infection timing by time of year. We also show how seasonal forcing can induce resonant dynamics that result in a cumulative infection burden that is greater (or lesser) than would arise in the absence of forcing. We end in Section 5 with a brief conclusion.

2 An immuno-epidemiological transmission model

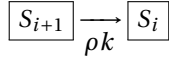
In this section, we construct an immuno-epidemiological model of respiratory virus transmission. We first classify our population of interest according to their epidemiological status, which may be either susceptible (S) or infectious (I). Individuals in the susceptible class have some effective antibody level c against the currently circulating virus. We assume that this level decays exponentially with time due to a combination of antibody waning and antigenic drift, yielding an effective antibody decay rate r .

For simplicity, we have taken here that any contribution of antigenic drift to the effective antibody decay rate is fixed over time. This is consistent with the approximately linear increase in antigenic distance over time observed in, for example, the influenza viruses (Bedford, Suchard, et al. 2014). However, it does not capture the possibility of antigenic variation increasing during times of greater viral transmission (Bedford, Riley, et al. 2015).

To capture this effective antibody level within a compartmental framework, we stratify the susceptible population across compartments S_i where $0 \leq i \leq k$, each with a corresponding effective antibody level c_i :

$$c_i = 2^{a(i/k)},$$

where the parameter a defines the maximal effective antibody level of 2^a . Here, we describe these levels using powers of two in line with the common use of two-fold serial dilution assays for the measurement of the antibody response (e.g. Salk 1944; Killian 2020). The exponential decay in effective antibody level is then captured using a method of lines approximation (Appendix A, Plant and Wilson 1986; Angelov et al. 2023), with individuals in compartment S_{i+1} moving to compartment S_i at a constant rate ρk :



for $i \geq 0$, where ρ is specified in terms of the desired effective antibody decay rate r :

$$\rho = \frac{r}{a \log_2 2}.$$

The parameter k controls the resolution of the stratification (with the model having $k+1$ strata over antibody level). Further, for individuals starting at the same antibody level, larger values of k reduce the degree of between-individual variation in effective antibody level following decay (Appendix A).

In sum, we have a population described across $k+2$ compartments:

$$\{S_0, S_1, \dots, S_k, I\},$$

with the value of each compartment describing the fraction of the population which is within each state, such that the value of all compartments sums to one.

Immune protection and viral transmission

We assume that individuals in the susceptible class have some level of immune protection against acquiring an infection with the currently circulating virus (conditional upon contact with an infected individual) which is dependent upon their effective antibody level. We take the protection ω_i for an individual in class S_i to be a dose-response relationship over this effective antibody level c_i , specifically a Hill equation with a mid-point c_{mid} and Hill coefficient b :

$$\omega_i = \frac{c_i^b}{c_{\text{mid}}^b + c_i^b}.$$

This dose-response relationship has been previously used in both epidemiological studies of antibody-mediated immune protection (Halloran et al. 2009; Khoury et al. 2021; Hogan et al. 2023; Hao et al. 2025) and dynamic models of transmission (Zachreson et al. 2023; Conway et al. 2024), though typically in the (mathematically equivalent) formulation of logistic regression over $\log c$. Here, we only consider the effect of antibodies in providing protection against acquiring infection, conditional upon contact with an infected individual. We do not consider other potential effects of antibody-mediated immunity, such as reducing the probability of developing severe disease or of transmitting the virus onwards.

In our model, contact between individuals occurs according to mass-action effect. A susceptible individual makes infectious contacts with infected individuals at a rate given by the product of the proportion of infectious individuals I and the infectiousness parameter β . Individuals in each susceptible strata S_i are then infected according to this rate of exposure, reduced by their level of antibody-mediated protection ω_i :

$$\boxed{S_i} \xrightarrow{(1-\omega_i)\beta I} \boxed{I}$$

Recovery from infection and post-infection immunity

Infectious individuals are assumed to recover from infection at a fixed rate γ (such that the mean duration of infectiousness is $1/\gamma$). Upon recovery from infection, individuals transition to a susceptible strata S_i according to the probability $P(I \rightarrow S_i)$:

$$\boxed{I} \xrightarrow{\gamma P(I \rightarrow S_i)} \boxed{S_i}$$

We specify $P(I \rightarrow S_i)$ in terms of an assumed distribution of effective antibody level following recovery from infection. Specifically, we take that the log-2-transformed value of the effective antibody level follows a Normal distribution with mean μ and standard deviation σ . This distribution then defines the probability of transitioning into each discrete susceptible strata, noting we have an additional constraint that antibody level must fall within the range $[2^0, 2^a]$:

$$P(I \rightarrow S_i) = \begin{cases} P(a < X), & i = k, \\ P\left(a \frac{i}{k} < X \leq a \frac{i+1}{k}\right), & i > 0 \text{ and } i < k, \\ P(X \leq a \frac{1}{k}), & i = 0. \end{cases}$$

The use of a Normal distribution here is consistent with observations of the antibody response following infection with respiratory viruses (Khoury et al. 2021).

The model of immunity we describe here captures only the first-order dynamics of antibody rise and decay within an individual. To simplify our analysis, we do not consider the dynamics of other components that make up the human adaptive immune response, such as plasma cells (which produce antibodies), memory B-cells (which recall the antibody response upon re-infection) or T-cells (which may provide protection independent of the antibody response). If these other components behaved in a similar manner to the antibody response but provided protection across greater durations, their presence could be seen as equivalent to a reduced decay rate r . However, more complex behaviour such as interactions between the different components across repeat infections cannot be captured by our one-dimensional model.

Further, we do not capture any process of demographic change in this model, which has been previously identified as an important factor in similar modelling studies (Dafilis et al. 2012). If this process were to act via the removal of individuals at random and the addition of immune-naive individuals, a greater rate of demographic turnover would be approximately equivalent to an increase in the effective antibody decay rate.

Model structure

Combining the above model transitions, we have a deterministic dynamical system defined by $k+2$ ordinary differential equations:

$$\frac{dS_i}{dt} = \begin{cases} -\beta(1-\omega_i)S_i I + \gamma P(I \rightarrow S_i)I & -\rho k S_i, \quad i = k, \\ -\beta(1-\omega_i)S_i I + \gamma P(I \rightarrow S_i)I + \rho k S_{i+1} - \rho k S_i, & 0 < i < k, \\ -\beta(1-\omega_i)S_i I + \gamma P(I \rightarrow S_i)I + \rho k S_{i+1}, & i = 0, \end{cases} \quad (1)$$

and

$$\frac{dI}{dt} = \beta I \sum_{i=0}^k (1-\omega_i)S_i - \gamma I, \quad (2)$$

which we illustrate in Figure 1. This model is similar in nature to the general recovery-stratified model described by El Khalifi and Britton (2023), but differs in our allowance for variability in the post-infection antibody level and their use of different functions to describe immune protection across the different strata.

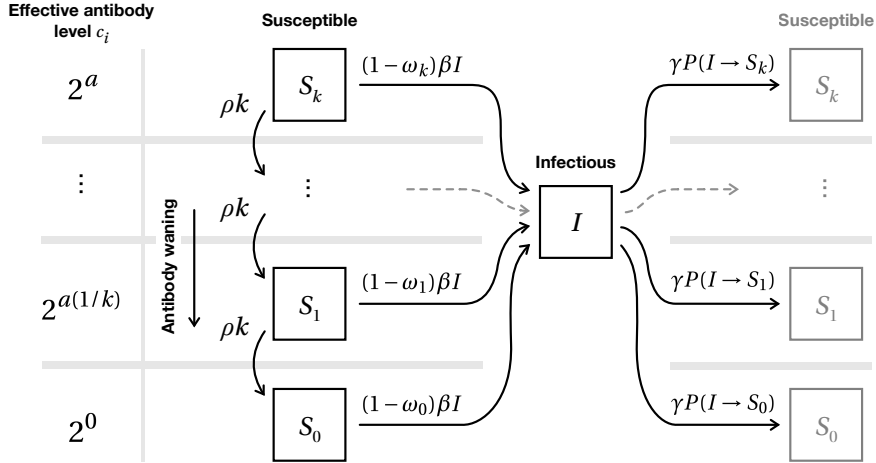


Figure 1: Compartmental flow diagram of our immuno-epidemiological model of respiratory virus transmission. The susceptible class S_i is stratified according to their effective antibody level c_i (which may range from 2^0 up to 2^a), with this defining ω_i , the level of immune protection against infection given contact with an infected individual.

Numerical methodology

All results were produced using the parameter values listed in Table 1 (except where the effective antibody decay rate r was otherwise varied). These values correspond to a moderately infectious respiratory virus with a basic reproduction number (R_0) of 1.5 and a generation interval of four days. At baseline, antibody-mediated protection was specified such that at least 50% protection from re-infection was maintained following recovery from infection for a median period of approximately 230 days. We set the initial conditions of the system such that a small proportion of the population was infectious ($I = 0.001$), while the remaining population was in the susceptible class at the minimum effective antibody level ($S_0 = 0.999$).

Where we calculated infection incidence (i.e. the number of new infections across some period), we included in our numerical implementation an additional cumula-

tive infections compartment C_I , defined as:

$$\frac{dC_I}{dt} = \beta I \sum_{j=0}^k (1 - \omega_j) S_j,$$

where daily infection incidence for day t is then calculated as $\text{inc}(t) = C_I(t+1) - C_I(t)$.

We identified the (stable or unstable) fixed points of the system by first reducing the systems dimensionality by taking $I = 1 - \sum_{i=0}^k S_i$ and setting the left hand side of this system to zero and solving for $\{S_0, S_1, \dots, S_k\}$ under the constraint that each compartment value was positive. A fixed point solution was defined as stable where all eigenvalues of the reduced linearised system had real components less than zero.

We assessed numerical solutions for chaos using the Melbourne 0-1 test across the numerically integrated infection prevalence time-series $I(t)$ following 1,000 years of burn-in (Gottwald and Melbourne 2016). To avoid known issues with the test regarding the oversampling of continuous-time dynamical systems, we performed the test over infection prevalence sampled once every 80 days. This downsampling rate was identified visually to achieve good classification performance over a subset of the results (Appendix Figure 9). To distinguish between periodic, quasiperiodic and chaotic solutions (and identify the duration of the periodic solutions), we used a classification algorithm which we describe in Appendix C.

All numerical analysis was performed in Julia (Bezanson et al. 2017). Numerical integration of the dynamical system was performed using the 5th order Rosenbrock-Wanner method *Rodas5P* as implemented in the *DifferentialEquations.jl* package (Rackauckas and Nie 2017; Steinebach 2023). *NonlinearSolve.jl* was used for identifying the fixed points of the system (Rackauckas, Pal, et al. 2023), and *DynamicalSystems.jl* was used for the Melbourne 0-1 test for chaos (Datseris 2018; Datseris and Parlitz 2022). Visualisation of results was performed in the R statistical computing environment using the *ggplot2* package (R Core 2013; Wickham 2011).

The code used to produce the results is available on GitHub (https://github.com/ruarai/ode_immunity) and has been archived on OSF (osf.io/us9t8).

| Parameter | Value |
|---|-----------------------------------|
| Maximum strata index | $k = 32$ |
| Maximal effective antibody level | $2^a = 2^{8.0}$ |
| Effective antibody decay rate (where otherwise unchanged) | $r = 0.015 \text{ days}^{-1}$ |
| Recovery rate | $\gamma = 0.25 \text{ days}^{-1}$ |
| Transmission rate | $\beta = 0.375 \text{ days}^{-1}$ |
| Post-infection antibody level | $X \sim N(6, 0.5)$ |
| Midpoint of the protection function | $c_{\text{mid}} = 2^3$ |
| Hill coefficient of the protection function | $b = 8$ |

Table 1: Model parameter values used in the results.

3 Model dynamics

We illustrate the characteristic dynamics produced by the transmission model in Figure 2, with parameters as specified in Table 1. Across the first 125 days, we observe an SIR-like wave of infection (Figure 2A), with over half of the population initially in S_0 being infected (Figure 2B). Following recovery from infection, the fraction of the population within the higher-index susceptible classes increases (Figure 2C), in line with the assumed distribution of post-infection effective antibody levels. The population then experiences antibody waning, with the fraction within the lower-index susceptible classes increasing. Once there is a sufficiently large density of susceptible individuals in lower-index (and lower-protection) classes, a subsequent wave of infection occurs. This cycle repeats indefinitely undamped. Such oscillatory behaviour

is typical of immuno-epidemiological models where the population is structured by immunity (Heffernan and M J Keeling 2009; Böhm et al. 2016; Barbarossa et al. 2018). We illustrate the complete distribution of individuals across the susceptible strata over time in Appendix Figure 1. The arithmetic mean of effective antibody level also varies substantially with time (Figure 2D). Starting at a mean of 2^0 (with all susceptible individuals in S_0), the initial wave of infection leads to a peak mean effective antibody level of approximately $2^{4.5}$, and between waves of infection the level reaches a minimum of around 2^2 .

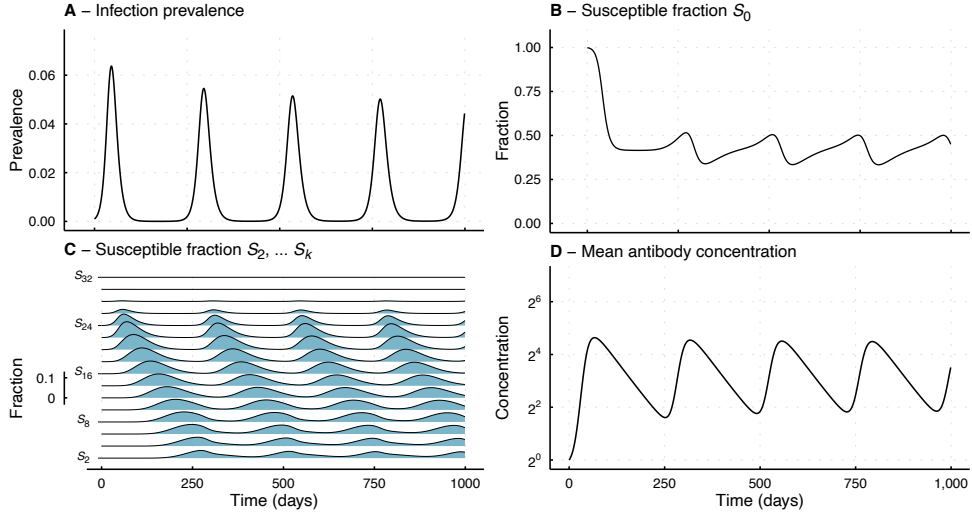


Figure 2: Characteristic dynamics of the immunity-structured model of respiratory virus transmission. Model parameters are as in Table 1. **A:** Prevalence (i.e. fraction) of infectious individuals I over time. **B:** Fraction of susceptible individuals in the minimum antibody strata S_0 . **C:** Fraction of susceptible individuals in the strata S_2 through to S_k (odd strata not plotted for visual clarity), with each strata plotted as an individual ribbon. **D:** The mean effective antibody level across the susceptible population, calculated as an arithmetic mean (i.e. not a geometric mean).

We now examine the effect of varying the effective antibody decay rate r . For the range of effective antibody decay rates explored ($0 < r \leq 0.05 \text{ days}^{-1}$), we observe a variety of dynamical outcomes (Figure 3A). For high values of decay rate (e.g. $r = 0.03$), infection prevalence tends towards a stable fixed point (e.g. Figure 3D panel iii). As the decay rate is reduced, a supercritical Hopf bifurcation occurs (at $r \approx 0.025 \text{ days}^{-1}$), with the fixed point solution becoming unstable and a stable periodic solution emerging (e.g. Figure 3D panel ii). This Hopf bifurcation is evident in a pair of conjugate eigenvalues of the linearised system crossing the imaginary axis (Appendix Figure 2). A similar Hopf bifurcation is identified in Hethcote et al. (1981), where periodic solutions arise in an SIRS delay-differential equation model. As the decay rate is reduced further, a second Hopf bifurcation occurs at $r \approx 0.005 \text{ days}^{-1}$, with the fixed point solution again becoming stable and the pair of conjugate eigenvalues returning to the left hand side of the complex plane (Appendix Figure 2). Following this second Hopf bifurcation, the periodic solution produced by the first Hopf bifurcation remains stable, implying the existence of a separatrix which divides the two basins of attraction between the stable periodic solution and the stable fixed point solution. We illustrate two trajectories in this regime ($r = 0.003 \text{ days}^{-1}$, Figure 3D panel i), one which tends towards the stable periodic solution and one which tends towards the stable fixed point solution.

We identify that the minimal infection prevalence across the stable periodic solution declines rapidly as the effective antibody decay rate r is decreased (Figure 3A). At the extremely low minimal infection prevalences that we observe (e.g. $I < 10^{-7}$), it would be expected that, in any realistic setting, the dynamics of transmission around this minimum would be highly stochastic. For example, in a population size of

10^8 , this would correspond to less than ten concurrent infections on average at the trough between each wave, implying a high probability of pathogen extinction. In this scenario, the sustained transmission of a virus would only be possible where the antibody-mediated immunity across the population could otherwise be avoided (e.g. through demographic change). However, the existence of a second Hopf bifurcation implies that a virus which induces a particularly slow decaying antibody response (less than $r \approx 0.005 \text{ days}^{-1}$) could evade extinction at the stable fixed point, where infection prevalence is relatively high.

We find that both the frequency of the stable periodic solution and the average annual infection incidence increase approximately linearly with effective antibody decay rate r (Figure 3B, C). This average annual infection incidence is calculated as the average daily infection incidence in the period following 100,000 days of burn-in, multiplied by 365. Notably, where both a fixed point solution and a stable periodic solution are present (r less than approximately 0.025 days^{-1}), this average annual infection incidence is equal between the two solutions.

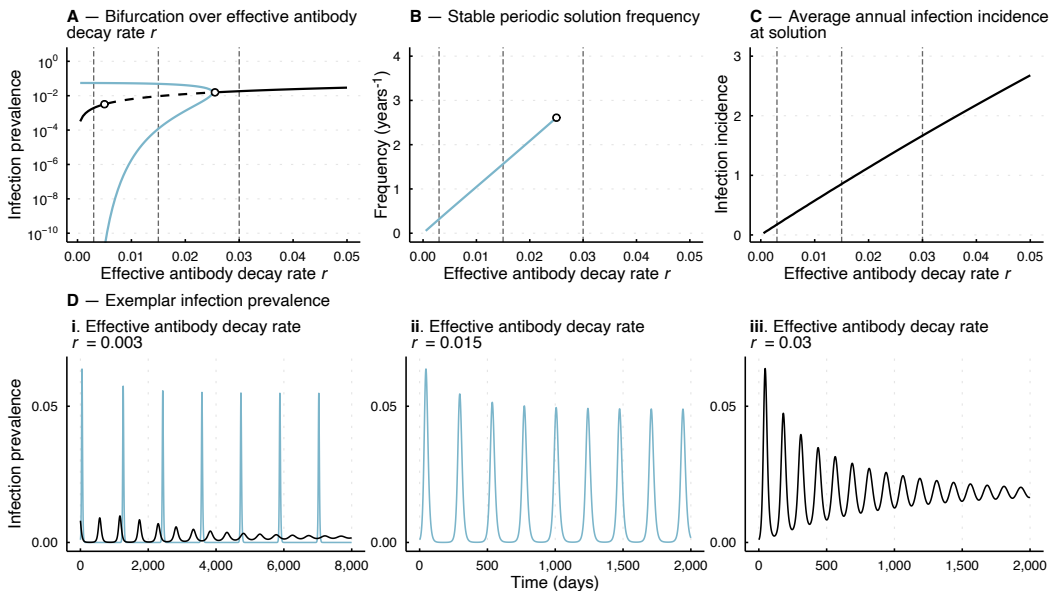


Figure 3: Dynamics of the immuno-epidemiological model for varying values of effective antibody decay rate r (all other model parameters are as in Table 1). The system was evaluated across a period of 100 years (36,500 days), following 100 years of burn-in. **A:** Bifurcation diagram over varying effective antibody decay rate r , with lines depicting infection prevalence at the model solutions (noting the log scale on the y-axis). For the periodic solutions, the light blue lines correspond to the maximal or minimal infection prevalence across each solution. For low values of the decay rate (e.g. less than $r = 0.01 \text{ days}^{-1}$), the minimal infection prevalence rapidly approaches values where stochastic effects would be dominant in realistic settings and our deterministic results must be interpreted with care. The separatrix between the stable limit cycle and the stable fixed point for values of r less than approximately 0.005 days^{-1} is not depicted as it could not be identified numerically. **B:** The frequency (in years $^{-1}$) of the periodic model solutions for varying effective antibody decay rate r . **C:** The average annual infection incidence at the model solution (across both fixed point and stable periodic solutions) across effective antibody decay rate r , calculated as the mean daily infection incidence multiplied by 365. **D:** Exemplar dynamics in infection prevalence across the three dynamical regimes, corresponding to the vertical dashed lines in A-C. Those which tend towards a stable periodic solution are illustrated in blue while those which tend towards a stable fixed point are black. The solution for $r = 0.003 \text{ days}^{-1}$ (panel i) which tends towards the stable fixed point was initialised by sampling a random point in state space near the fixed point. Note that the x-axis extent differs for panel i.

Stratification of the infectious class and antibody boosting

In Appendix B, we provide a specification of the model where the infectious class is also stratified by effective antibody level. In this version of the model, a susceptible individual in S_i who is infected enters the corresponding infectious compartment

I_i . Infectious individuals then recover and return to a susceptible compartment S_j according to a probability distribution $P(I_i \rightarrow S_j)$. This allows us to specify a dependence between the pre-infection and post-infection effective antibody level c_i and c_j .

We use this model to examine the effect of ‘antibody boosting’, where an individual’s post-infection effective antibody level is an increasing function of their pre-infection effective antibody level (Barbarossa et al. 2018; Diekmann et al. 2018). Our results (Appendix Figure 7) show that the inclusion of antibody boosting may quantitatively alter the dynamics produced by the model, changing both the peak infection prevalence and peak mean effective antibody level. However, the overall qualitative nature of the dynamics are unchanged. As in Figure 3, we identify two Hopf bifurcations across the effective antibody decay rate, an (approximate) linear relationship between the decay rate and the periodic solution frequency, and an (approximate) linear relationship between the decay rate and the average annual infection incidence. Given the lack of qualitative differences in equilibrium dynamics, in the following sections we consider the model without stratification of the infectious class.

4 Waning, seasonal forcing and periodicity

In this section, we extend the model to include a seasonally-varying transmission rate and examine how this affects the long-term epidemiological dynamics. To do this, we consider a time-varying infectiousness term:

$$\beta(t) = \beta_0 \left(1 + \eta \cos\left(\frac{2\pi}{365}t\right) \right),$$

such that infectiousness varies sinusoidally over a period of 365 days, with a maximal value of $\beta_0(1 + \eta)$ at the start of each year, and a minimal value of $\beta_0(1 - \eta)$ mid-year (corresponding to seasonal effects in a temperate region in the Northern Hemisphere). In the following, we take $\beta_0 = 0.375$, such that the average value of $\beta(t)$ matches the constant β used in the previous section.

Across values of the effective antibody decay rate r ranging from zero (no antibody decay) to 0.1 (high decay rate) and values of the strength of seasonal forcing η ranging from zero (no seasonal forcing) to 0.5 (very high seasonal forcing), a diverse range of long-term dynamics are identified (Figure 4A). This includes periodic solutions (with periods of one or more years), quasiperiodic solutions and chaotic dynamics, where we have defined chaos as a positive result on the Melbourne 0-1 test (Appendix C).

Across this parameter space, the occurrence of periodic solutions is dependent upon the natural period of the system (i.e. the period in the absence of seasonal forcing, $\eta = 0$). In Figure 4A, we annotate the y-axis with this natural period for a subset of rational multiples of the one-year period of seasonal forcing. As the seasonal forcing strength η is increased from zero, periodic solutions appear in triangular clusters around these rational multiples, with the period in years of the solution equal to the numerator of the rational multiple. These regions are known as ‘Arnold tongues’ (Datseris and Parlitz 2022). Each rational multiple of the natural period has a corresponding Arnold tongue, however, only a small number are visible in our visualisation as they typically become vanishingly small as the numerator or denominator increases (Datseris and Parlitz 2022). The presence of these Arnold tongues implies that — for certain effective decay rates — periodicity in infection dynamics could be induced by mechanisms which only have slight effects upon the rate at which the virus may be transmitted across each year. For example, even a 10% difference in the rate at which individuals make contact between the summer and winter periods of the year (i.e. $\eta \approx 0.05$) leads to periodicity across a wide range of effective antibody decay rates. This identification of high sensitivity of periodicity to seasonal forcing aligns with similar findings made using a stochastic SIRS model with an exponentially distributed period of immunity (Dushoff et al. 2004).

In the space bounded between these Arnold tongues, and for effective antibody decay rates less than 0.025 days^{-1} (where, in the absence of seasonal forcing, stable periodic solutions are present), quasiperiodic solutions can be identified (e.g. Figure 4B, panel ii). For these quasiperiodic solutions, the duration of time between each wave of infection is relatively predictable, but the timing of these waves shifts relative to the calendar year each year, such that epidemics may peak at any time of year in the long-run (Appendix Figure 5). Hypothetically, a newly emergent respiratory virus could exhibit such quasiperiodic dynamics in the long-term if it were to become endemic within the human population. This could present a challenge to public health planning, as any strategies predicated upon the regular seasonal recurrence of an epidemic would be undermined. Public health activities such as pathogen surveillance, vaccination deployment, and the mobilisation of healthcare workers — rather than beginning and ending on an approximately regular calendar schedule — would need to be adjusted each year, and would often fall outside the winter epidemic season. However, epidemics that occur outside of the usual wintertime period are less likely to be co-circulating with other viruses, and hence the total clinical load from respiratory infections might be lower compared to winter months.

As the seasonal forcing strength η increases, the growing Arnold tongues collide with one another, and regions of chaotic dynamics are evident. Period-doubling bifurcations can be identified at the border of some of these chaotic regions (Appendix Figure 9). Notably, the presence of chaos does not necessarily imply that the long-term qualitative dynamics of infection are difficult to anticipate or manage. For example, the trajectory exhibiting chaotic dynamics that we present (Figure 4D, panel v) exhibits relatively little variation in the timing and magnitude of the primary (larger) wave of infection each year. Rather, the effects of chaos are more pronounced in the secondary (smaller) wave of infection, which has a size that varies substantially year to year.

The minimum infection prevalence we observe (across the 250 years following burn-in) varies substantially across the same parameter space (Figure 4B). The minimum infection prevalence has the highest value where seasonal forcing is absent and the effective antibody decay rate is greatest (i.e. $\eta = 0$ and $r = 0.03 \text{ days}^{-1}$), and tends to reduce as either the strength of seasonal forcing η is increased or the effective antibody decay rate r is decreased. The minimum infection prevalence drops substantially in the Arnold tongue corresponding to the natural period of one year. Generally, results where seasonal forcing is present have substantially lower values of minimum infection prevalences than those without forcing (Appendix Figure 3). As in the case without seasonal forcing, the results which reach particularly low infection prevalence would, in realistic settings, have greater probabilities of stochastic extinction occurring.

We find that the rate at which peaks in infection incidence occur across the period following burn-in may vary widely as the strength of seasonal forcing and the effective antibody decay rate change (Appendix Figure 4A, B). Recent work by Rubin et al. (2025) has investigated the possibility that the ‘sub-annual’ recurrence of SARS-CoV-2 — in which multiple waves of infection occur each year — which has been observed in many regions could be driven by the dynamics of immunity. We identify similar results, with lower effective antibody decay rates yielding multiple peaks in infection incidence per year following burn-in (Appendix Figure 4B).

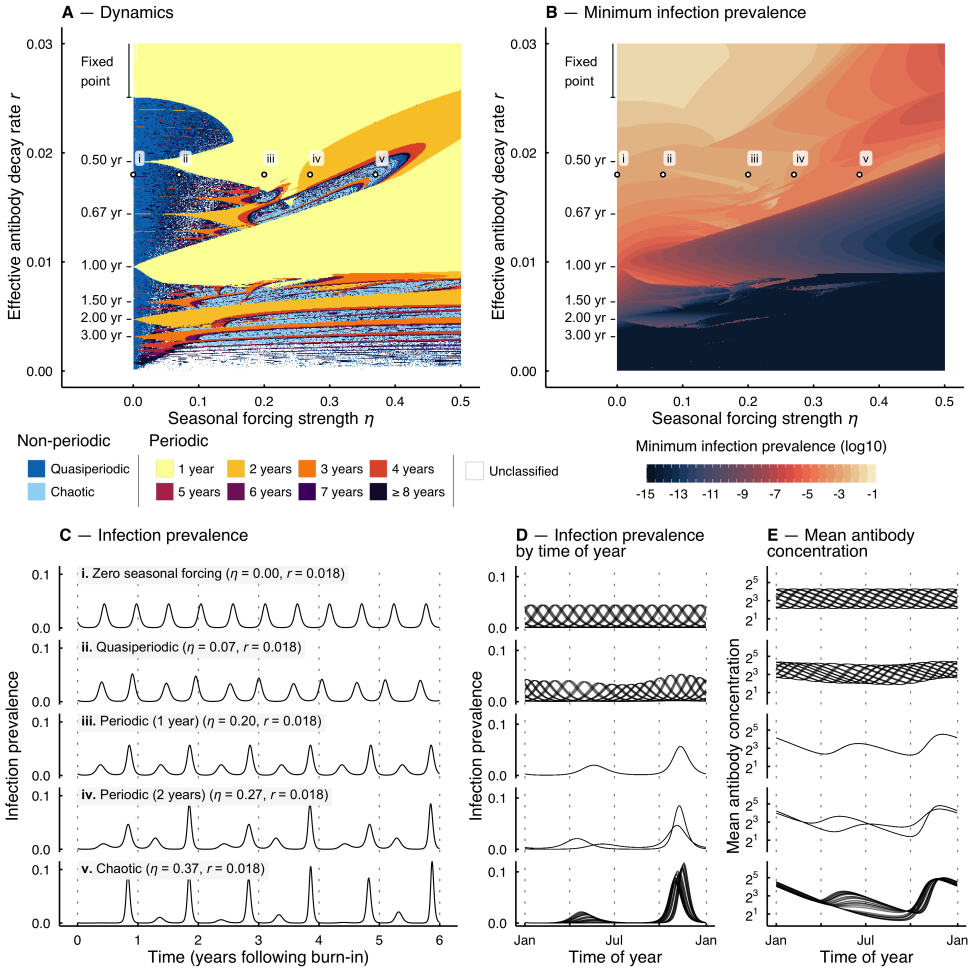


Figure 4: Model dynamics across varied seasonal forcing strength η and effective antibody decay rate r . Model parameters are otherwise as in Table 1. The system was evaluated across a period of 250 years, following 1,000 years of burn-in. **A:** The qualitative dynamics yielded following burn-in for each parameter pair. Our approach to classifying the dynamics of the numerically integrated model solutions is described in Appendix C. **B:** The minimum infection prevalence across the 250 years following burn-in for each parameter pair. For realistic settings, results with a low minimum (e.g. less than 10^{-7}) would likely be dominated by stochastic effects. **C:** Example trajectories of infection prevalence across six years following burn-in. **D, E:** Example trajectories of infection prevalence and mean effective antibody level respectively, indexed by time of year. Trajectories from 60 consecutive years following burn-in are displayed.

The exemplar dynamics described above demonstrate that the timing of infection incidence across each year may vary substantially across different values of the effective antibody decay rate r and seasonal forcing strength η . We now examine this further, identifying the distribution of infection timing by time of year across the same parameter space. We summarise this distribution using the circular mean and variance, quantities which account for the cyclic nature of the calendar year (Appendix D). The mean timing of infection is most often located around the start/end of the year (Figure 5A), coinciding with when seasonal forcing is greatest. However, there is substantial heterogeneity in this mean, with many parameter combinations yielding an earlier mean infection timing around October (e.g. Figure 5C, panel ii) or a later mean around April (e.g. Figure 5C panel iv).

The circular variance also varies substantially across the parameter space (Figure 5B). The lowest circular variance is observed for parameters which fall into Arnold tongues which have a corresponding natural period greater than one year. In the tongues, the resultant dynamics of infection exhibit strong seasonality, with the majority of infections occurring across a short period of each year (e.g. Figure 5C

panels **iii** and **iv**). Outside of the tongues, the circular variance is highly dependent upon the strength of forcing η . Where the strength of seasonal forcing is high (e.g. $\eta \geq 0.25$), the circular variance is intermediate and the apparent seasonality of infections is less pronounced (e.g. Figure 5C panel **ii**). For low values of forcing, the circular variance approaches one, implying that (in the long-run) dynamics are highly aseasonal and infections with the virus may occur at any time of year (e.g. Figure 5C panel **i**).

These results align with the commonly observed seasonality of respiratory viruses in temperate regions, where different viruses are observed to be most prevalent at different times of the year (Moriyama et al. 2020). For example, the influenza viruses and respiratory syncytial virus are most prevalent during the wintertime, while rhinovirus is most prevalent during autumn and spring (Moriyama et al. 2020; Kimberlin et al. 2021). Although such differences could arise due to differences in the rate at which the different viruses are transmitted across the course of each year (i.e. different seasonal forcing functions) or interference between the pathogens (Nickbakhsh et al. 2019), our results show that large differences in the timing of infections throughout the year could arise solely from differences in the human immune response to the virus or the ability of the virus to evade prior immunity.

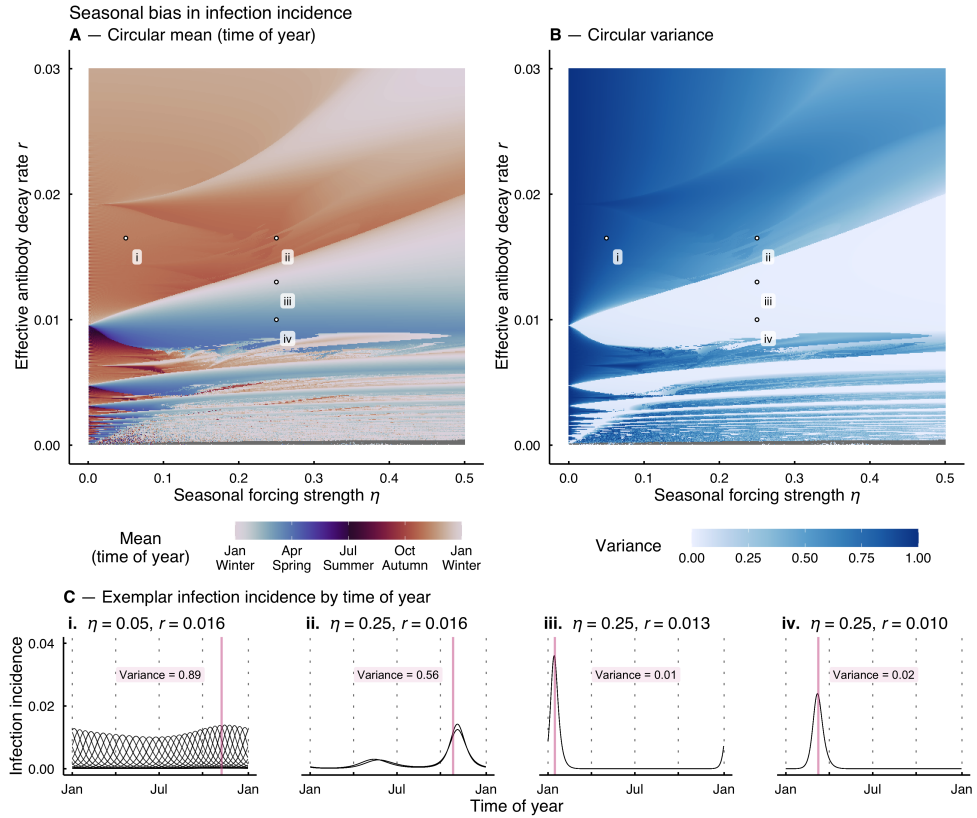


Figure 5: The seasonal bias in the time of infection across varied seasonal forcing strength η and effective antibody decay rate r . Parameters are otherwise as in Table 1. Calculation of the circular mean and variance is detailed in Appendix D. The system was evaluated across a period of 250 years, following 1,000 years of burn-in. **A:** The circular mean of time of year of infection incidence. **B:** The circular variance in time of year of infection incidence, which ranges between zero (entirely concentrated at one day of the year) and one (completely uniform across the year). **C:** Exemplar infection incidence trajectories by time of year (following burn-in), corresponding to the points *i* through *iv* depicted on the panels above. Trajectories are displayed across 60 years following burn-in. For each model solution, we illustrate both the circular mean (vertical line) and circular variance (text).

Finally, we identify that seasonal forcing can induce resonant amplification (or damping) which yields infection burdens greater (or lesser) than would otherwise

occur in the absence of forcing. We illustrate this by calculating the average annual infection incidence (i.e. the mean daily incidence in the period following burn-in multiplied by 365) for varying effective antibody decay rate r and seasonal forcing strength η (Figure 6). For weak seasonal forcing ($\eta = 0.1$) the resultant average annual infection incidence differs little from the baseline. However, as the strength of seasonal forcing η is increased to 0.3 or 0.5, the annual average infection incidence changes substantially (Figure 6). For the high seasonal forcing case of $\eta = 0.5$, burden is approximately 20% larger than baseline for an effective antibody decay rate of $r = 0.01 \text{ days}^{-1}$. At this decay rate, the system has a natural frequency (i.e. in the absence of seasonal forcing, $\eta = 0$) of approximately one period per year (Figure 3B), i.e. the forcing frequency and the natural frequency are very similar. Conversely, at a decay rate of $r = 0.02 \text{ days}^{-1}$, the average annual infection burden is reduced by approximately 25%. At this decay rate, the system has a natural frequency of around two periods per year, such that forcing is often acting in opposition to the natural oscillatory behaviour of the system.

These results show that the interaction between seasonal forcing and waning immunity not only shapes the timing of infections but can produce substantial differences in the long-term average infection burden of a respiratory virus. These differences are large enough that models would fail to predict the long-term public health impact of a respiratory virus if they did not capture this interaction. While we do not consider vaccination in our model, the presence of such resonant dynamics could have significant implications for the design of vaccination programs, as recurring annual vaccination programs could act as an additional driver of immuno-epidemiological resonance (Choisy et al. 2006).

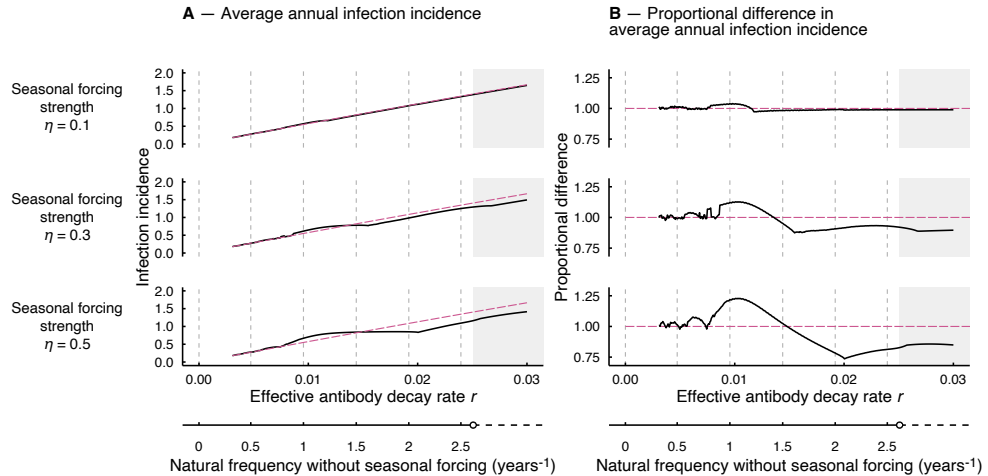


Figure 6: Changes in infection burden due to resonant dynamics induced by seasonal forcing, across varied effective antibody decay rate r . All other parameters as listed in Table 1. The corresponding natural frequency of the system (i.e. without seasonal forcing) is displayed as a secondary axis. Grey shading illustrates values of effective antibody decay rate that would go to a fixed point solution in the absence of seasonal forcing. The system was evaluated across a period of 250 years, following 1,000 years of burn-in. **A:** The average annual infection incidence following burn-in across effective antibody decay rate and increasing seasonal forcing strength η . The dashed pink line indicates the average annual infection incidence in the absence of seasonal forcing ($\eta = 0$, as in Figure 3C) **B:** The proportional difference in the average annual infection incidence following burn-in for the given value of seasonal forcing strength η compared to the zero seasonal forcing case ($\eta = 0$).

5 Conclusions

We have examined the influence of antibody-mediated immunity upon the seasonality of respiratory viruses by constructing an immuno-epidemiological model of respiratory virus transmission, where an individual's level of immune protection

against (re-)infection is dependent upon their effective antibody level, which decays with some combination of antibody waning and antigenic drift. Using this model, we have found that periodic epidemic waves can arise in the absence of seasonal forcing and have identified two associated Hopf bifurcations across the effective antibody decay rate. Where seasonal forcing is included in the model, we have shown that diverse dynamical outcomes can arise. These include periodic dynamics, which resemble the annual (or multi-annual) seasonal epidemics of endemic respiratory viruses in temperate regions (Moriyama et al. 2020), and chaotic dynamics, which we have found can still exhibit (in the qualitative sense) seasonal behaviour. We have also identified a regime of quasiperiodicity, with epidemic waves recurring at a regular interval but never aligning with the calendar year in the long-term, a pattern not present in public health surveillance data of respiratory viruses. These different dynamical regimes produce varying patterns of infection timing by time-of-year, and this timing varies with the interaction between the effective antibody decay rate and seasonal forcing. Beyond shaping the seasonality of infection timing, we find this interaction can produce a resonant amplification or damping, leading to non-linear changes in the long-term infection burden as a function of the effective antibody decay rate.

The modelling framework we have presented could be extended to capture the concurrent transmission of multiple viral strains where each strain imparts a cross-reactive antibody response. This kind of cross-reactive immunity, typically arising as a consequence of antigenic shift (rather than the antigenic drift we have captured with the effective antibody decay rate here), can be found among many respiratory viruses (Sullender 2000; Carter et al. 2013; Koutsakos and Ellebedy 2023). Such an extension would involve the inclusion of multiple infected classes and a (multi-dimensional) stratification of the susceptible class by the antibody level imparted by each strain, with this allowing for immune protection due to prior infection to be specified in terms of antibody cross-reactivity (unlike previously published multi-strain models that use relative cross-protection values, e.g. Gupta et al. 1996; Andreasen et al. 1997; Kucharski et al. 2016). This multi-strain model could be used to explore, for example, the transmission dynamics of influenza, for which cross-reactivity between sub-types of influenza is likely a key driver (Andreasen et al. 1997; Carter et al. 2013; Krammer 2019). Such a multi-strain model could also be used to explore the phenomena of antibody-dependent enhancement, where the presence of cross-reactive antibodies can lead to a heightened susceptibility to infection or worsened disease outcomes (Wells et al. 2025).

Investigating the dynamics of any particular respiratory virus with our model would require careful parametrisation of transmission, immunity and seasonal forcing. Given appropriate parametrisation, such an analysis would enable the exploration of the biological plausibility of the different dynamic behaviours that we have highlighted (such as quasiperiodicity or resonant amplification). Further, such a parametrised study could be of particular value in application to SARS-CoV-2. While early modelling studies predicted that the virus would, in the long-term, approach a stable pattern of once-a-year winter seasonality in temperate regions (e.g. Kissler et al. 2020; Townsend et al. 2023), the virus does not yet appear to have fallen into this pattern in many temperate regions, with off-winter waves continuing to be observed (Donovan et al. 2025; Rubin et al. 2025; UK Health Security Agency 2025). Our results highlight how a variety of seasonal patterns beyond that of once-a-year winter seasonality — such as quasiperiodic waves that do not align with the calendar year — could emerge as the long-term behaviour of a respiratory virus like SARS-CoV-2 as a natural consequence of the interaction between the periodic drivers of waning immunity and seasonal forcing.

6 Acknowledgements

We thank Cameron Zachreson for their helpful input on this research. Ruarai Tobin was supported by a Melbourne Research Scholarship. This research was also supported by The University of Melbourne’s Research Computing Services and the Petascale Campus Initiative.

7 Funding

James McCaw was supported by an ARC Laureate Fellowship (FL240100126). Freya Shearer was supported by an NHMRC Investigator Grant (Emerging Leader Fellowship, 2021/GNT2010051). These funders had no role in study design, collection, analysis and interpretation of data, writing of the report or decision to submit the article for publication.

References

- Altizer, Sonia et al. (Apr. 2006). “Seasonality and the dynamics of infectious diseases: Seasonality and infectious diseases”. en. In: *Ecol. Lett.* 9.4, pp. 467–484. issn: 1461-023X,1461-0248. doi: [10.1111/j.1461-0248.2005.00879.x](https://doi.org/10.1111/j.1461-0248.2005.00879.x).
- Andraud, Mathieu et al. (Mar. 2012). “Living on three time scales: the dynamics of plasma cell and antibody populations illustrated for hepatitis a virus”. en. In: *PLoS Comput. Biol.* 8.3, e1002418. issn: 1553-7358,1553-734X. doi: [10.1371/journal.pcbi.1002418](https://doi.org/10.1371/journal.pcbi.1002418).
- Andreasen, V, J Lin, and S A Levin (Aug. 1997). “The dynamics of cocirculating influenza strains conferring partial cross-immunity”. en. In: *J. Math. Biol.* 35.7, pp. 825–842. issn: 0303-6812,1432-1416. doi: [10.1007/s002850050079](https://doi.org/10.1007/s002850050079).
- Angelov, G et al. (2023). *An immuno-epidemiological model with waning immunity after infection or vaccination*. Tech. rep. TU Wien.
- Barbarossa, Maria Vittoria, M Polner, and G Röst (Aug. 2018). “Temporal evolution of immunity distributions in a population with waning and boosting”. en. In: *Complexity* 2018, pp. 1–13. issn: 1076-2787,1099-0526. doi: [10.1155/2018/926474](https://doi.org/10.1155/2018/926474) 3.
- Bedford, Trevor, Steven Riley, et al. (July 2015). “Global circulation patterns of seasonal influenza viruses vary with antigenic drift”. en. In: *Nature* 523.7559, pp. 217–220. issn: 0028-0836,1476-4687. doi: [10.1038/nature14460](https://doi.org/10.1038/nature14460).
- Bedford, Trevor, Marc A Suchard, et al. (Feb. 2014). “Integrating influenza antigenic dynamics with molecular evolution”. en. In: *eLife* 3, e01914. issn: 2050-084X. doi: [10.7554/eLife.01914](https://doi.org/10.7554/eLife.01914).
- Bezanson, Jeff et al. (Jan. 2017). “Julia: A fresh approach to numerical computing”. en. In: *SIAM Rev. Soc. Ind. Appl. Math.* 59.1, pp. 65–98. issn: 0036-1445,1095-7200. doi: [10.1137/141000671](https://doi.org/10.1137/141000671).
- Böhm, Axel, Nikolaos Stilianakis, and Andreas Widder (2016). *Optimal Control of Infectious Diseases in a Population with Heterogeneous Dynamic Immunity*.
- Carter, Donald M et al. (Feb. 2013). “Sequential seasonal H1N1 influenza virus infections protect ferrets against novel 2009 H1N1 influenza virus”. en. In: *J. Virol.* 87.3, pp. 1400–1410. issn: 0022-538X,1098-5514. doi: [10.1128/JVI.02257-12](https://doi.org/10.1128/JVI.02257-12).
- Choisy, Marc, Jean-François Guégan, and Pejman Rohani (Nov. 2006). “Dynamics of infectious diseases and pulse vaccination: Teasing apart the embedded resonance effects”. en. In: *Physica D* 223.1, pp. 26–35. issn: 0167-2789,1872-8022. doi: [10.1016/j.physd.2006.08.006](https://doi.org/10.1016/j.physd.2006.08.006).
- Conway, Eamon et al. (May 2024). “Optimal timing of booster doses in a highly vaccinated population with minimal natural exposure to COVID-19”. In: *bioRxiv*, p. 2024.05. 14.24307386. doi: [10.1101/2024.05.14.24307386](https://doi.org/10.1101/2024.05.14.24307386).

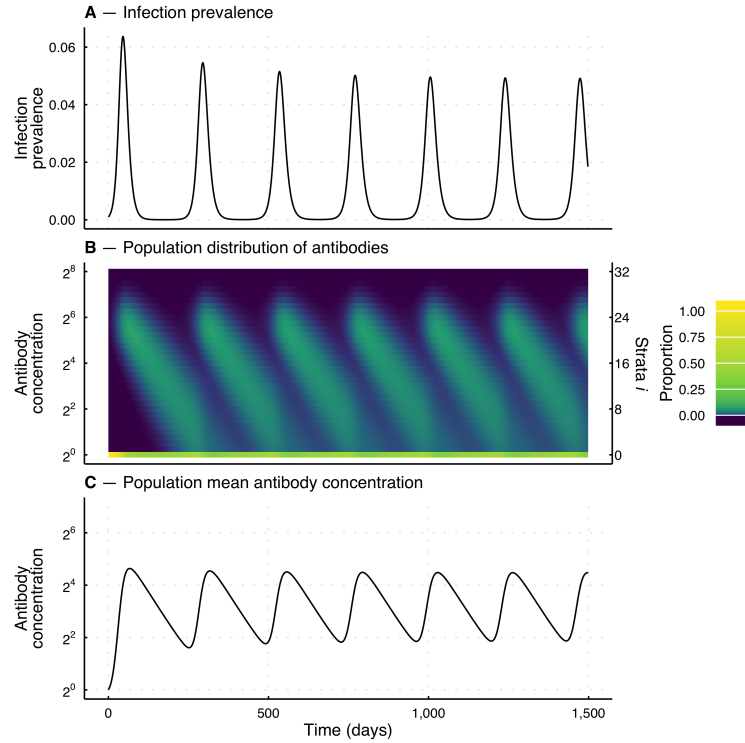
- Coudeville, Laurent et al. (Mar. 2010). "Relationship between haemagglutination-inhibiting antibody titres and clinical protection against influenza: development and application of a bayesian random-effects model". en. In: *BMC Med. Res. Methodol.* 10.1, p. 18. issn: 1471-2288,1471-2288. doi: 10.1186/1471-2288-10-18.
- Dafilis, M P et al. (Oct. 2012). "The influence of increasing life expectancy on the dynamics of sirs systems with immune boosting". en. In: *ANZIAM J. Electron. Suppl.* 54.1-2, pp. 50–63. issn: 1446-1811,1446-8735. doi: 10.1017/s1446181113000023.
- Datseris, George (Mar. 2018). "DynamicalSystems.jl: A Julia software library for chaos and nonlinear dynamics". In: *J. Open Source Softw.* 3.23, p. 598. issn: 2475-9066. doi: 10.21105/joss.00598.
- Datseris, George and Ulrich Parlitz (Mar. 2022). *Nonlinear dynamics: A concise introduction interlaced with code*. en. 1st ed. Undergraduate Lecture Notes in Physics. Cham, Switzerland: Springer Nature. isbn: 9783030910310,9783030910327. doi: 10.1007/978-3-030-91032-7.
- Diekmann, O et al. (Dec. 2018). "Waning and boosting: on the dynamics of immune status". en. In: *J. Math. Biol.* 77.6-7, pp. 2023–2048. issn: 0303-6812,1432-1416. doi: 10.1007/s00285-018-1239-5.
- Donovan, Ash et al. (Oct. 2025). *Australian Respiratory Surveillance Report — 22 September to 5 October 2025*. Tech. rep. Interim Australian Centre for Disease Control.
- Dushoff, Jonathan et al. (Nov. 2004). "Dynamical resonance can account for seasonality of influenza epidemics". en. In: *Proc. Natl. Acad. Sci. U. S. A.* 101.48, pp. 16915–16916. issn: 0027-8424,1091-6490. doi: 10.1073/pnas.0407293101.
- El Khalifi, Mohamed and Tom Britton (Sept. 2023). "Extending susceptible-infectious-recovered-susceptible epidemics to allow for gradual waning of immunity". en. In: *J. R. Soc. Interface* 20.206, p. 20230042. issn: 1742-5689,1742-5662. doi: 10.1098/rsif.2023.0042.
- Gottwald, Georg A and Ian Melbourne (2016). "The 0-1 Test for Chaos: A Review". In: *Chaos Detection and Predictability*. Lecture notes in physics. Berlin, Heidelberg: Springer Berlin Heidelberg, pp. 221–247. isbn: 9783662484081,9783662484104. doi: 10.1007/978-3-662-48410-4__7.
- Gupta, S et al. (Apr. 1996). "The maintenance of strain structure in populations of recombining infectious agents". en. In: *Nat. Med.* 2.4, pp. 437–442. issn: 1078-8956,1546-170X. doi: 10.1038/nm0496-437.
- Halloran, M Elizabeth, Ira M Longini, and Claudio Jose Struchiner (Nov. 2009). *Design and analysis of vaccine studies*. en. 2010th ed. Statistics for Biology and Health. New York, NY: Springer. isbn: 9780387403137. doi: 10.1007/978-0-387-68636-3.
- Hao, Tianxiao et al. (Mar. 2025). "Predicting immune protection against outcomes of infectious disease from population-level effectiveness data with application to COVID-19". en. In: *Vaccine* 55.126987, p. 126987. issn: 0264-410X,1873-2518. doi: 10.1016/j.vaccine.2025.126987.
- Heffernan, J M and M J Keeling (June 2009). "Implications of vaccination and waning immunity". en. In: *Proc. Biol. Sci.* 276.1664, pp. 2071–2080. issn: 0962-8452,1471-2954. doi: 10.1098/rspb.2009.0057.
- Hethcote, Herbert W, Harlan W Stech, and P Van Den Driessche (Feb. 1981). "Non-linear oscillations in epidemic models". In: *SIAM J. Appl. Math.* 40.1, pp. 1–9. issn: 0036-1399,1095-712X. doi: 10.1137/0140001.
- Hobson, D et al. (Dec. 1972). "The role of serum haemagglutination-inhibiting antibody in protection against challenge infection with influenza A2 and B viruses". en. In: *J. Hyg. (Lond.)* 70.4, pp. 767–777. issn: 0022-1724,2396-8184. doi: 10.1017/s0022172400022610.
- Hogan, Alexandra B et al. (July 2023). "Estimating long-term vaccine effectiveness against SARS-CoV-2 variants: a model-based approach". en. In: *Nat. Commun.* 14.1, p. 4325. issn: 2041-1723,2041-1723. doi: 10.1038/s41467-023-39736-3.
- Iuliano, A Danielle et al. (Mar. 2018). "Estimates of global seasonal influenza-associated respiratory mortality: a modelling study". en. In: *Lancet* 391.10127, pp. 1285–1300. issn: 0140-6736,1474-547X. doi: 10.1016/S0140-6736(17)33293-2.

- Keeling, Matt J and Pejman Rohani (Jan. 2008). *Modeling infectious diseases in humans and animals*. Princeton: Princeton University Press. ISBN: 9781400841035. doi: 10.1515/9781400841035.
- Khoury, David S et al. (July 2021). "Neutralizing antibody levels are highly predictive of immune protection from symptomatic SARS-CoV-2 infection". en. In: *Nat. Med.* 27.7, pp. 1205–1211. ISSN: 1078-8956,1546-170X. doi: 10.1038/s41591-021-01377-8.
- Killian, Mary Lea (2020). "Hemagglutination assay for influenza virus". en. In: *Methods Mol. Biol.* 2123, pp. 3–10. ISSN: 1940-6029,1064-3745. doi: 10.1007/978-1-0716-0346-8_1.
- Kim, Hyunsuh, Robert G Webster, and Richard J Webby (Mar. 2018). "Influenza virus: Dealing with a drifting and shifting pathogen". en. In: *Viral Immunol.* 31.2, pp. 174–183. ISSN: 0882-8245,1557-8976. doi: 10.1089/vim.2017.0141.
- Kimberlin, David W et al. (2021). *Red Book: 2018-2021 report of the committee on infectious diseases*. American Academy of Pediatrics. doi: 10.5555/20183376718.
- Kissler, Stephen M et al. (May 2020). "Projecting the transmission dynamics of SARS-CoV-2 through the postpandemic period". en. In: *Science* 368.6493, pp. 860–868. ISSN: 0036-8075,1095-9203. doi: 10.1126/science.abb5793.
- Koutsakos, Marios and Ali H Ellebedy (May 2023). "Immunological imprinting: Understanding COVID-19". en. In: *Immunity* 56.5, pp. 909–913. ISSN: 1074-7613,1097-4180. doi: 10.1016/j.immuni.2023.04.012.
- Krammer, Florian (June 2019). "The human antibody response to influenza A virus infection and vaccination". en. In: *Nat. Rev. Immunol.* 19.6, pp. 383–397. ISSN: 1474-1733,1474-1741. doi: 10.1038/s41577-019-0143-6.
- Kucharski, Adam J, Viggo Andreasen, and Julia R Gog (Jan. 2016). "Capturing the dynamics of pathogens with many strains". en. In: *J. Math. Biol.* 72.1-2, pp. 1–24. ISSN: 0303-6812,1432-1416. doi: 10.1007/s00285-015-0873-4.
- Li, You et al. (May 2022). "Global, regional, and national disease burden estimates of acute lower respiratory infections due to respiratory syncytial virus in children younger than 5 years in 2019: a systematic analysis". en. In: *Lancet* 399.10340, pp. 2047–2064. ISSN: 0140-6736,1474-547X. doi: 10.1016/S0140-6736(22)00478-0.
- London, W P and J Yorke (Dec. 1973). "Recurrent outbreaks of measles, chickenpox and mumps. I. Seasonal variation in contact rates". In: *Am. J. Epidemiol.* 98.6, pp. 453–468. ISSN: 0002-9262,1476-6256. doi: 10.1093/oxfordjournals.aje.a121575.
- Medina, Rafael A and Adolfo García-Sastre (July 2011). "Influenza A viruses: new research developments". en. In: *Nat. Rev. Microbiol.* 9.8, pp. 590–603. ISSN: 1740-1526,1740-1534. doi: 10.1038/nrmicro2613.
- Moriyama, Miyu, Walter J Hugentobler, and Akiko Iwasaki (Sept. 2020). "Seasonality of respiratory viral infections". en. In: *Annu. Rev. Virol.* 7.1, pp. 83–101. ISSN: 2327-056X,2327-0578. doi: 10.1146/annurev-virology-012420-022445.
- Msemburi, William et al. (Jan. 2023). "The WHO estimates of excess mortality associated with the COVID-19 pandemic". en. In: *Nature* 613.7942, pp. 130–137. ISSN: 0028-0836,1476-4687. doi: 10.1038/s41586-022-05522-2.
- Murphy, Kenneth M and Casey Weaver (Mar. 2019). *Janeway's Immunobiology, 9th Edition*. en. <https://www.wileydirect.com.au/blog/buy/janeways-immunobiology/>. Accessed: 2025-3-4.
- Nelson, Randy J (Apr. 2004). "Seasonal immune function and sickness responses". en. In: *Trends Immunol.* 25.4, pp. 187–192. ISSN: 1471-4906,1471-4981. doi: 10.1016/j.it.2004.02.001.
- Nickbakhsh, Sema et al. (Dec. 2019). "Virus-virus interactions impact the population dynamics of influenza and the common cold". en. In: *Proc. Natl. Acad. Sci. U. S. A.* 116.52, pp. 27142–27150. ISSN: 0027-8424,1091-6490. doi: 10.1073/pnas.1911083116.
- Phillips, Daniel J et al. (July 2024). "Improved estimates of COVID-19 correlates of protection, antibody decay and vaccine efficacy waning: a joint modelling

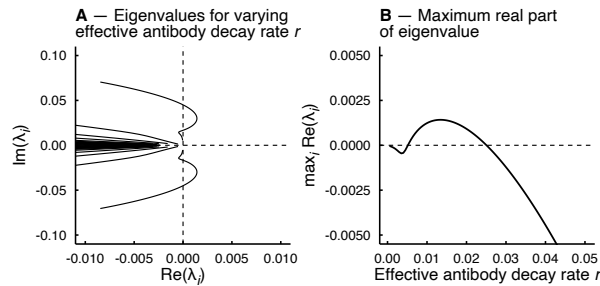
- approach". en. In: *bioRxiv*, p. 2024.07.02.24309776. doi: [10.1101/2024.07.02.24309776](https://doi.org/10.1101/2024.07.02.24309776).
- Plant, R E and L T Wilson (1986). "Models for age structured populations with distributed maturation rates". en. In: *J. Math. Biol.* 23.2, pp. 247–262. issn: 0303-6812,1432-1416. doi: [10.1007/bf00276960](https://doi.org/10.1007/bf00276960).
- R Core (2013). "R: A language and environment for statistical computing". In: *Foundation for Statistical Computing, Vienna, Austria*.
- Rackauckas, Christopher and Qing Nie (May 2017). "DifferentialEquations.Jl – A performant and feature-rich ecosystem for solving differential equations in Julia". en. In: *J. Open Res. Softw.* 5.1, p. 15. issn: 2049-9647,2049-9647. doi: [10.5334/jors.151](https://doi.org/10.5334/jors.151).
- Rackauckas, Christopher, Avik Pal, et al. (2023). *SciML/NonlinearSolve.jl: v3.1.1*. doi: [10.5281/ZENODO.10397607](https://doi.org/10.5281/ZENODO.10397607).
- Rubin, Ilan N et al. (June 2025). "Seasonal forcing and waning immunity drive the sub-annual periodicity of the COVID-19 epidemic". en. In: *medRxiv*, p. 2025.03.05.25323464. doi: [10.1101/2025.03.05.25323464](https://doi.org/10.1101/2025.03.05.25323464).
- Salk, Jonas E (Aug. 1944). "A simplified procedure for titrating hemagglutinating capacity of influenza-virus and the corresponding antibody". en. In: *J. Immunol.* 49.2, pp. 87–98. issn: 0022-1767,1550-6606. doi: [10.4049/jimmunol.49.2.87](https://doi.org/10.4049/jimmunol.49.2.87).
- Steinebach, Gerd (June 2023). "Construction of Rosenbrock–Wanner method Rodas5P and numerical benchmarks within the Julia Differential Equations package". en. In: *BIT* 63.2, pp. 1–26. issn: 0006-3835,1572-9125. doi: [10.1007/s10543-023-00967-x](https://doi.org/10.1007/s10543-023-00967-x).
- Sullender, W M (Jan. 2000). "Respiratory syncytial virus genetic and antigenic diversity". en. In: *Clin. Microbiol. Rev.* 13.1, pp. 1–15. issn: 0893-8512,1098-6618. doi: [10.1128/cmr.13.1.1-15.2000](https://doi.org/10.1128/cmr.13.1.1-15.2000).
- Susswein, Zachary, Eva C Rest, and Shweta Bansal (Apr. 2023). "Disentangling the rhythms of human activity in the built environment for airborne transmission risk: An analysis of large-scale mobility data". en. In: *eLife* 12. issn: 2050-084X. doi: [10.7554/eLife.80466](https://doi.org/10.7554/eLife.80466).
- Townsend, Jeffrey P et al. (Nov. 2023). "Seasonality of endemic COVID-19". en. In: *MBio*, e0142623. issn: 2161-2129,2150-7511. doi: [10.1128/mbio.01426-23](https://doi.org/10.1128/mbio.01426-23).
- UK Health Security Agency (Oct. 2025). *National flu and COVID-19 surveillance report: 23 October 2025 (week 43)*. en. Tech. rep.
- Webster, R (1999). "Antigenic variation in influenza viruses". In: *Contributions to microbiology and immunology* 8, pp. 377–390. doi: [10.1016/B978-012220360-2/50015-5](https://doi.org/10.1016/B978-012220360-2/50015-5).
- Webster, Robert G (Jan. 1999). "Antigenic Variation in Influenza Viruses". In: *Origin and Evolution of Viruses*. Elsevier, pp. 377–390. isbn: 9780122203602. doi: [10.1016/B978-012220360-2/50015-5](https://doi.org/10.1016/B978-012220360-2/50015-5).
- Wells, Timothy J et al. (Jan. 2025). "Mechanisms of antibody-dependent enhancement of infectious disease". en. In: *Nat. Rev. Immunol.* 25.1, pp. 6–21. issn: 1474-1733,1474-1741. doi: [10.1038/s41577-024-01067-9](https://doi.org/10.1038/s41577-024-01067-9).
- Wickham, Hadley (Mar. 2011). "Ggplot2: Ggplot2". en. In: *Wiley Interdiscip. Rev. Comput. Stat.* 3.2, pp. 180–185. issn: 1939-5108,1939-0068. doi: [10.1002/wics.147](https://doi.org/10.1002/wics.147).
- Zachreson, Cameron et al. (Oct. 2023). "Individual variation in vaccine immune response can produce bimodal distributions of protection". en. In: *Vaccine* 41.45, pp. 6630–6636. issn: 0264-410X,1873-2518. doi: [10.1016/j.vaccine.2023.09.025](https://doi.org/10.1016/j.vaccine.2023.09.025).

Appendix

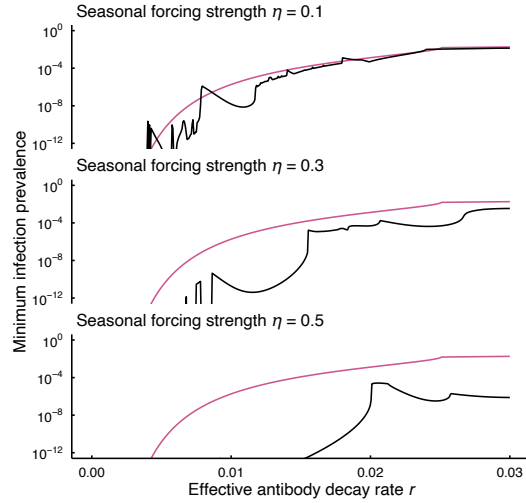
Appendix Figures



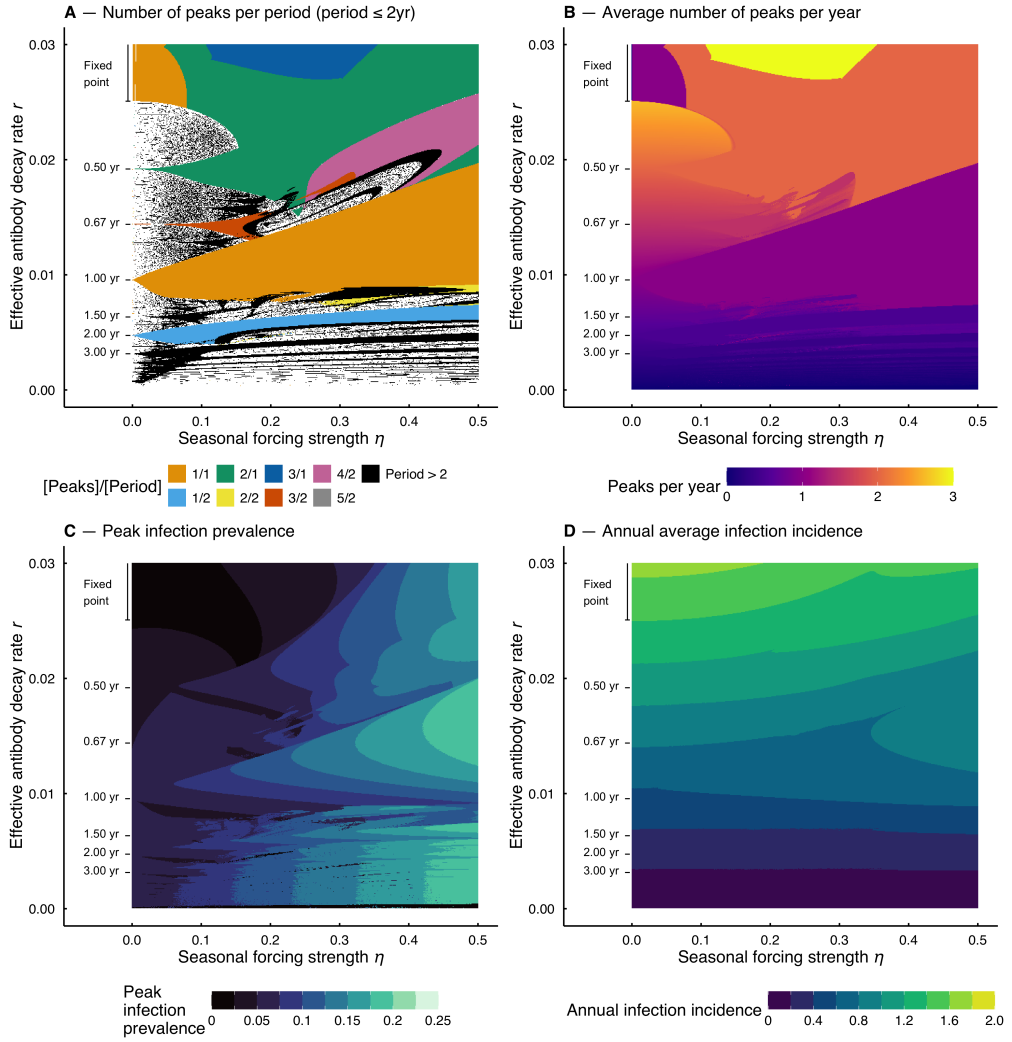
Appendix Figure 1: Characteristic dynamics of the immunity-structured model of respiratory virus transmission. Model parameters are as in Table 1. **A:** Prevalence (i.e. proportion) of infectious individuals I over time. **B:** Proportion of susceptible individuals in each strata S_i for $0 \leq i \leq k$. **C:** The mean antibody concentration across the susceptible population, calculated as an arithmetic mean across concentrations (i.e. not a geometric mean).



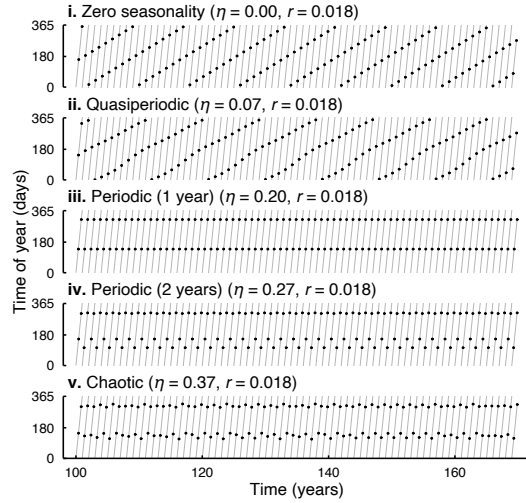
Appendix Figure 2: Eigenvalues of the linearised ODE system at the fixed point solution as antibody decay rate r is varied from 0 to 0.15. The linearised system was reduced by taking $I = 1 - \sum_{i=0}^k S_i$. **A:** Path of the eigenvalues λ_i as decay rate is varied. **B:** Maximal real part of the eigenvalues. Two Hopf bifurcations occur as this value crosses the x-axis.



Appendix Figure 3: The minimum infection prevalence observed for varying antibody decay rate r and strength of seasonal forcing η , where all other parameters are as in Table 1. The black line indicates the minimum infection prevalence for the specified value of η , while the red line indicates the minimum infection prevalence in the absence of seasonal forcing ($\eta = 0$). The system was evaluated across a period of 250 years, following 1,000 years of burn-in.



Appendix Figure 4: Differences in model dynamics across varied seasonal forcing strength η and antibody decay rate r . Model parameters are otherwise as in Table 1. Extends Figure 4 in the main text. The system was evaluated across a period of 250 years, following 1,000 years of burn-in. As in Figure 4, the natural period of the system in the absence of seasonal forcing ($\eta = 0$) is indicated on the left-hand side of each plot. **A:** The number of peaks per period duration (where period is at most two years). **B:** The average number of peaks per year across the 250 years following burn-in. **C:** Peak infection prevalence across the 250 years following burn-in. **D:** The average annual infection incidence across the 250 years following burn-in.



Appendix Figure 5: Timing of peak infection incidence (following 100 years of burn-in) for five exemplar sets of parameters (the same as those in Figure 5). Points indicate the timing of peak infection incidence by time of year (y-axis) and year (x-axis). Diagonal lines indicate the progression of time.

Appendix A

Compartmental approximation for the exponential decay in antibody concentration

Here, we derive the compartmental model of exponential decay in the susceptible population which is used in Section 2. We assume that individuals have some antibody concentration $c(t)$ which decays exponentially over time with decay rate r :

$$\frac{dc}{dt} = -rc(t).$$

This may be equivalently stated as a linear decay in the log-2-transformed concentration:

$$\frac{d\log_2(c)}{dt} = -\frac{r}{\log_e(2)}. \quad (3)$$

To capture this process across the population of susceptible individuals, we use a partial differential equation. Let $S(t, \log_2(c))$ be the fraction of susceptible individuals at time t who have a log-2 antibody concentration of $\log_2(c)$. From Equation 3, we have:

$$\frac{\partial S}{\partial t} - \frac{r}{\log_e(2)} \frac{\partial S}{\partial \log_2(c)} = 0 \quad (4)$$

We may approximate this PDE using the method of lines (e.g. Plant and Wilson 1986). First, we discretise antibody concentration across discrete strata i , taking:

$$c_i = 2^{a(i/k)}, \quad (5)$$

where $0 \leq i \leq k$ (such that $2^0 \leq c_i \leq 2^a$). The partial derivative of S with respect to $\log_2(c)$ is then approximately:

$$\frac{\partial S}{\partial \log_2(c)} \approx \frac{S_{i+1} - S_i}{\log_2(c_{i+1}) - \log_2(c_i)} = \frac{S_{i+1} - S_i}{a/k}$$

Substituting this approximation into our partial differential equation (Equation 4) yields:

$$\frac{dS_i}{dt} = \frac{rk}{a\log_e(2)} (S_{i+1} - S_i)$$

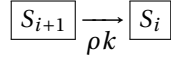
To simplify the equation, we take:

$$\rho = \frac{r}{a\log_e 2},$$

such that we have

$$\frac{dS_i}{dt} = \rho k (S_{i+1} - S_i).$$

This yields our compartmental approximation of the antibody decay process, with individuals in compartment S_{i+1} transitioning to compartment S_i at rate ρk :



for $i > 0$.

The parameter k controls the resolution of our approximation of Equation 4, with increasing k reducing the variance in the antibody decay process across the population. To show this, we note that the probability of an individual having made i transitions by time t is given by the Poisson distribution $I(t) \sim \text{Poisson}(\rho kt)$ (where we are ignoring the possibility of reaching the minimum strata). Assuming that all individuals in the population start at $t = 0$ with the same antibody concentration,

the change in $\log_2(c(t))$ across the population following $I(t)$ transitions is then (using Equation 5):

$$-\frac{aI(t)}{k},$$

which is distributed with a variance of:

$$\text{Var}\left(-\frac{aI(t)}{k}\right) = \frac{a^2\rho}{k}t.$$

As such, increasing k produces a more accurate approximation of the continuous decay process by reducing the variance introduced by discretisation.

Appendix B

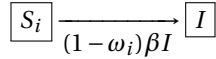
Transmission model with stratification across the infectious class.

Here, we consider a formulation of our transmission model where we stratify both the susceptible and infectious class by their serum antibody concentration (i.e. not only the susceptible class). This allows us to specify a post-infection antibody concentration with dependence upon the pre-infection antibody concentration. We use this to examine antibody boosting, where recovery from infection leads to a linear increase in the log-transformed antibody concentration.

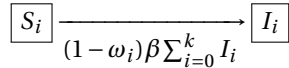
This model has $2(k+1)$ compartments:

$$\{S_0, S_1, \dots, S_k, I_0, I_1, \dots, I_k\},$$

and the process of antibody waning occurs as in the original model, with:

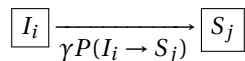


Infection occurs in a similar manner to the original model, although the force of infection is now calculated across the sum of the infectious compartments, i.e. $\beta \sum_{i=0}^k I_i$. Upon infection, an individual in S_i transitions to compartment I_i (i.e. the same strata index i):



where ω_i is the level of protection against infection (given exposure) for strata i , as defined in the main text.

Upon recovery from infection, an individual in compartment I_i may transition to any compartment S_j where $j \geq i$. This occurs according to the probability $P(I_i \rightarrow S_j)$, i.e.:



As in the original model, this probability may be defined to capture different mechanisms. Here, we consider a model of antibody boosting, where the log-concentration of antibodies following infection $\log_2(c_{\text{post}})$ increases linearly with the pre-infection concentration $\log_2(c_{\text{pre}})$, i.e.:

$$\log_2(c_{\text{post}}) = \log_2(c_{\text{pre}}) + X$$

where $X \sim N(\mu, \sigma)$ is a Normal distribution defining the jump in log-concentration. This defines the probabilities $P(I_i \rightarrow S_j)$:

$$P(I_i \rightarrow S_j) = \begin{cases} P(a \leq X), & j = k, \\ P(a \frac{i}{k} < X \leq a \frac{i+1}{k}), & i > j \text{ and } j < k, \\ P(X < a \frac{i+1}{k}), & j = i, \end{cases}$$

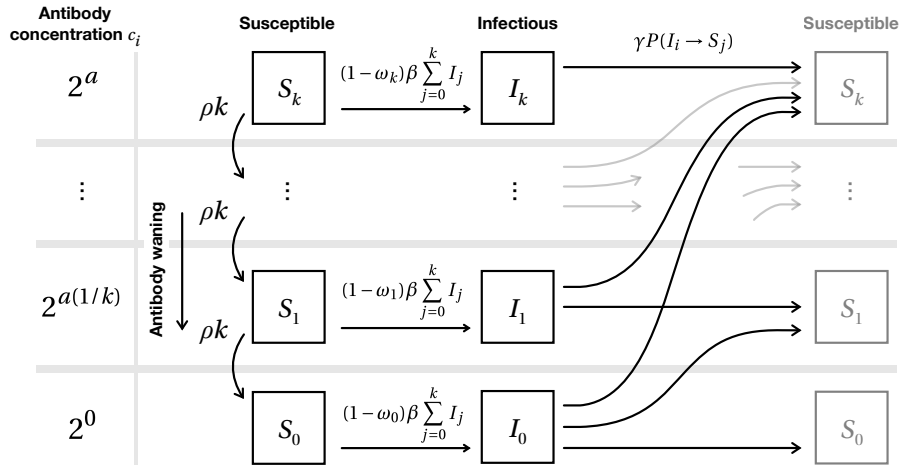
where we have applied the additional constraints that antibody concentration cannot decrease and may not be above 2^a . In the below results, we have taken $X \sim N(6, 0.5)$, such that the distribution of post-infection antibody concentration is approximately the same as in the main text where pre-infection antibody concentration is minimal (2^0).

In total, we have the following dynamical system defined by $2(k+1)$ ordinary differential equations:

$$\frac{dS_i}{dt} = \rho k ([i < k] S_{i+1} - [i > 0] S_i) - \beta (1 - \omega_i) S_i \sum_{j=0}^k I_j + \gamma \sum_{j=0}^k I_j P(I_j \rightarrow S_i)$$

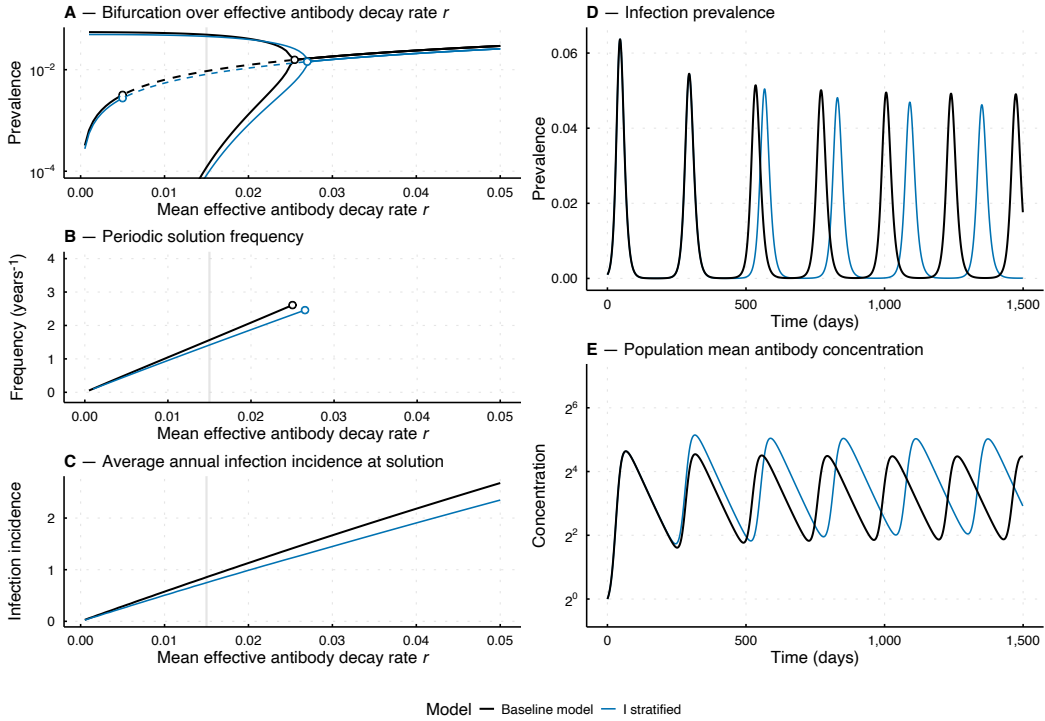
$$\frac{dI_i}{dt} = \beta (1 - \omega_i) S_i \sum_{j=0}^k I_j - \gamma I_i,$$

which is illustrated in Figure 6.



Appendix Figure 6: Diagram of the immuno-epidemiological model with stratification across both the susceptible and infectious classes.

Here, we compare the behaviour of this model with antibody boosting to that of the original model in the absence of seasonal forcing (Figure 7). The bifurcation diagram presented in Figure 7A illustrates a slight difference in the location of the fixed point and periodic solutions (and accompanying bifurcations). Similarly, both the frequency of the periodic solutions and the average annual infection incidence following burn-in are slightly lower for the model with boosting than the original model (Figure 7B). This similarity is also apparent in the exemplar trajectories of infection prevalence (Figures 7D), while clearer differences can be seen in the underlying population average antibody concentration (Figure 7E).



Appendix Figure 7: Dynamics of the immuno-epidemiological model for varying values of antibody decay rate r (all other model parameters are as in Table 1). The system was evaluated across a period of 100 years (36,500 days), following 100 years of burn-in. **A:** Bifurcation diagram over varying antibody decay rate r , with lines depicting infection prevalence at the model solutions (noting the log scale on the y-axis). For the periodic solutions, the light blue lines correspond to the maximal or minimal infection prevalence across each solution. For low values of antibody decay rate, the minimal infection prevalence rapidly approaches values where stochastic effects would be dominant in realistic settings and our deterministic results must be interpreted with care. The separatrix between the stable limit cycle and the stable fixed point for values of r less than approximately 0.005 is not depicted as it could not be identified numerically. **B:** The frequency (years^{-1}) of the periodic model solutions for varying antibody decay rate r . **C:** The average annual infection incidence at the model solution (fixed point or stable periodic) for antibody decay rate r , calculated as the mean infection incidence multiplied by 365. These average annual infection incidences correspond to both the periodic and (unstable or stable) fixed point solutions. **D:** Exemplar infection prevalence $I(t)$ for the two models, where we have taken $r = 0.015$. **E:** Exemplar population mean antibody concentration for the same system as in panel D.

Appendix C

Algorithm to determine qualitative dynamics

In this section, we describe the numerical method we used to determine the qualitative dynamics of a solution, producing (approximate) classifications across between periodicity, quasiperiodicity and chaos. We also provide our method for determining the period length of a periodic solution.

We first attempt to determine the period length (where it exists). Let $\mathbf{x}(t) = \{S_0(t), S_1(t), \dots, S_k(t), I(t)\}$ be the state of our system at time t . We consider the system for time-points t separated by a time-step of Δt between t_0 and t_{\max} , i.e.

$$t \in [t_0, t_0 + \Delta t, t_0 + 2\Delta t, \dots, t_{\max}]$$

where t_0 is a time-point such that model transients are minimal (i.e. following some burn-in period) and t_{\max} is the final time-point of our model solution. For our results, we have taken a time-step of $\Delta t = 0.25$.

By definition, in the absence of external forcing (i.e. seasonal forcing), at least one period will have occurred between the times t_0 and $t_i > t_0$ if $\mathbf{x}(t_0) = \mathbf{x}(t_i)$. To account

for numerical error in our solutions of $\mathbf{x}(t)$, we take this as occurring where:

$$\|\mathbf{x}(t_i) - \mathbf{x}(t_0)\| < \epsilon$$

where $\epsilon = 10^{-6}$ for this manuscript. This condition is illustrated for an example model solution in Figure 8.

To identify period length, we first identify the time-points $t_0 < t_i < t_{\max}$ for which the above condition is fulfilled. Where we identify consecutive time-points, we replace each group of consecutive time-points with their central (mean) value. Let $T = [t_1, \dots, t_n]$ be the ordered array of time-points we identify in this manner. This is then used to calculate samples of period duration p_i :

$$p_i = \frac{t_i - t_0}{i},$$

with the mean of these samples forming our estimate of the period \bar{p} .

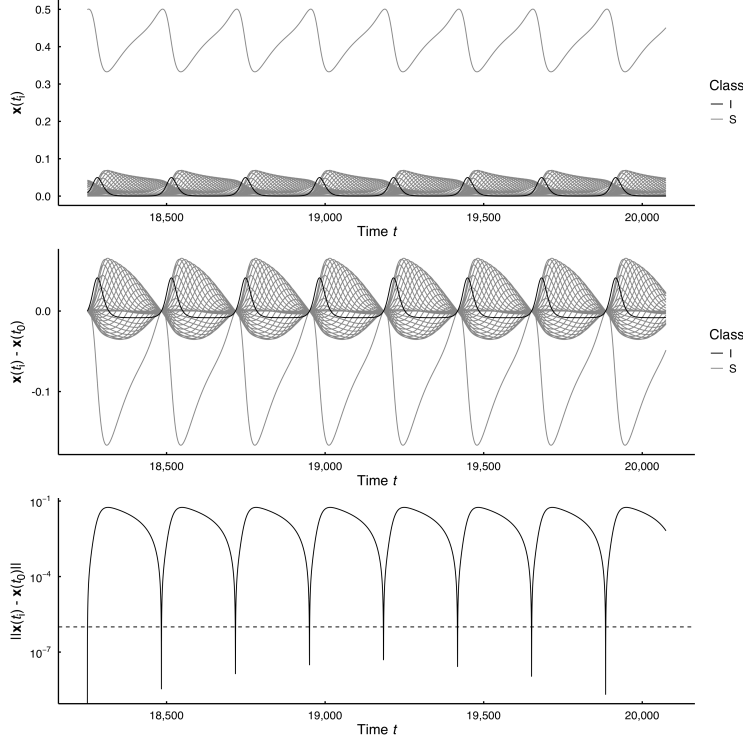
In the absence of seasonal forcing, we define a periodic solution as occurring where we have at least two samples of p_i and the standard deviation across p_i is less than one.

In the presence of seasonal forcing, we define a periodic solution as occurring where we have at least two samples of p_i and the mean period \bar{p} is such that the corresponding frequency is approximately a harmonic of 365 days, i.e.:

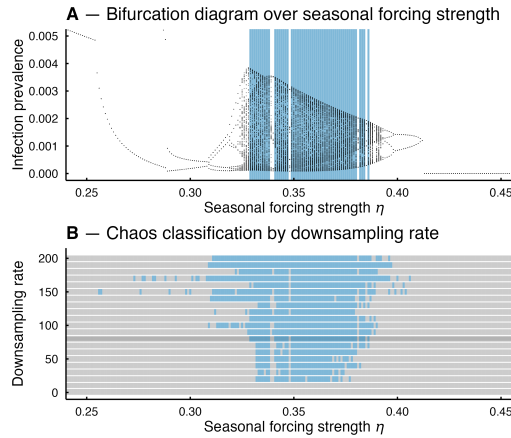
$$\exists n \in \{1, 2, \dots, 20\} \text{ such that } \min \{\text{mod}(n \cdot \bar{p}, 365), 365 - \text{mod}(n \cdot \bar{p}, 365)\} < 1.$$

The factor n allows us to periods at a minimum of 1/20 years. However, where seasonal forcing was present, we did not identify any such sub-annual periodic solutions.

Solutions where seasonal forcing is present can also be classified as chaotic or quasiperiodic. We define a (non-periodic) model solution to be chaotic where a value greater than 0.5 is returned by the Melbourne 0-1 test (Datseris 2018), with this test performed across infection prevalence sampled once every 80 days following burn-in. This value of 80 days was visually identified as achieving an acceptable classification performance (Appendix Figure 9). Dynamics which are identified as not chaotic or periodic may be classified as quasiperiodic if we have at least two samples of p_i but the value of \bar{p} is not a multiple or sub-multiple of 365 days (as defined above). Model solutions which do not fulfil one of these listed criteria will remain unclassified, which may occur where we have particularly long transient periods that prevent a periodic or quasiperiodic solution from being identified or the chaos test returns a false-negative result.



Appendix Figure 8: Illustration of the condition used to determine period occurrence. Top: The distance $\mathbf{x}(t_i) - \mathbf{x}(t_0)$ across each compartment making up the state \mathbf{x} . Trajectories are illustrated following burn-in. Bottom: The Euclidean distance $\|\mathbf{x}(t_i) - \mathbf{x}(t_0)\|$, with a horizontal dashed line indicating the threshold for period occurrence ($\epsilon = 10^{-6}$), noting that the y-axis is on a log-scale.



Appendix Figure 9: **A:** Bifurcation diagram over seasonality strength η , with effective decay rate fixed at $r = 0.018 \text{ days}^{-1}$. Period-doubling bifurcations are evident before chaotic behaviour emerges. Blue shading indicates where we have classified dynamics as chaotic using the Melbourne 0-1 test applied to the infection prevalence time-series downsampled at a rate of 80 days. **B:** Sensitivity analysis of the downsampling rate of the infection prevalence time-series to identify chaos. Blue shaded regions indicate where the Melbourne 0-1 test for chaos returned a value greater than 0.5 for that combination of seasonality strength η and downsampling rate. The row indicating the 80 day downsampling rate used in the manuscript is highlighted.

Appendix D

Circular statistics for seasonal bias calculations

We calculate circular statistics of mean and variance weighted by the daily infection

incidence time-series over time t (following burn-in) $\text{inc}(t)$ (where the calculation of incidence is described in the numerical methodology). We provide an illustration of this process in Figure 10 and detail the calculations in the following. To begin, we show how a time-point t may be represented as a vector on the unit circle (where this circle represents the year, or 365 days, and corresponds to the phase and period of the seasonal forcing). We may calculate the time-of-year t_{mod} of t in days between 0 and 364:

$$t_{\text{mod}} = \text{mod}(t, 365).$$

This time-of-year corresponds to an angle θ counter-clockwise around the unit circle (Figure 10):

$$\theta = \frac{2\pi t_{\text{mod}}}{365}.$$

And a corresponding vector (x, y) along the unit circle:

$$x = \cos(\theta), \quad y = \sin(\theta),$$

or equivalently:

$$x = \cos\left(\frac{2\pi}{365} \text{mod}(t, 365)\right), \quad y = \sin\left(\frac{2\pi}{365} \text{mod}(t, 365)\right).$$

Using the above definition, we may calculate the mean vector (\bar{x}, \bar{y}) of time-of-infection, weighting by the daily infection incidence $\text{inc}(t)$:

$$\begin{aligned}\bar{x} &= \frac{\sum_{t \in T} \text{inc}(t) \cos\left(\frac{2\pi}{365} \text{mod}(t, 365)\right)}{\sum_{t \in T} \text{inc}(t)} \\ \bar{y} &= \frac{\sum_{t \in T} \text{inc}(t) \sin\left(\frac{2\pi}{365} \text{mod}(t, 365)\right)}{\sum_{t \in T} \text{inc}(t)}\end{aligned}$$

where T is the sequence in days between the start of the post-burn-in period and the end of our numerical solution (where these must both be multiples of 365 such that only full years are included). We then calculate the circular mean day of year of infection \bar{d} as:

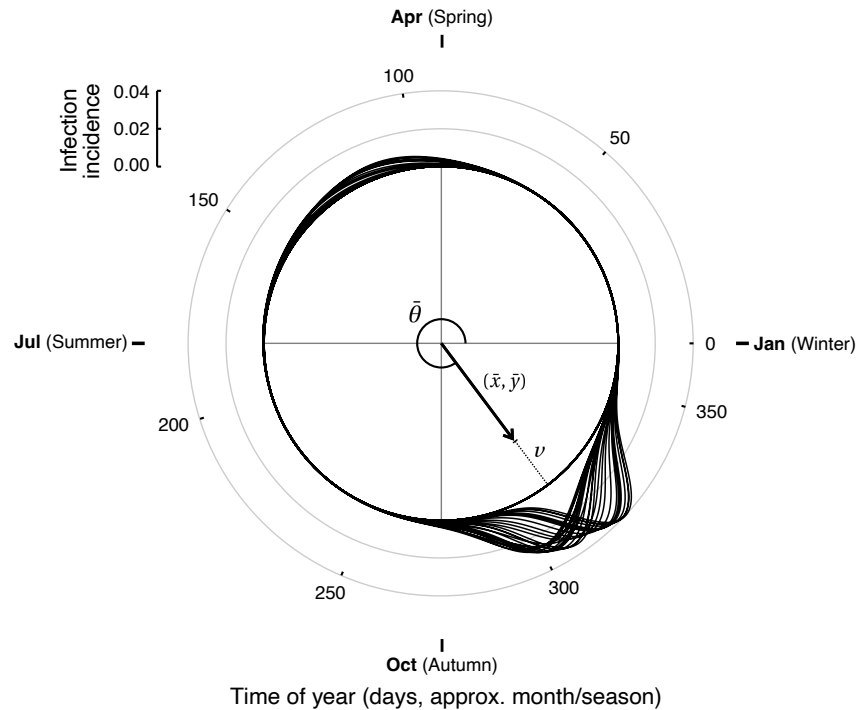
$$\bar{\theta} = \begin{cases} \text{atan2}(y = \bar{y}, x = \bar{x}) & \bar{y} \geq 0 \\ \text{atan2}(y = \bar{y}, x = \bar{x}) + 2\pi & \bar{y} < 0 \end{cases}$$

$$\bar{d} = \frac{365}{2\pi} \bar{\theta},$$

and the circular variance as one minus the magnitude of the mean vector:

$$\nu = 1 - \sqrt{\bar{x}^2 + \bar{y}^2}$$

which takes a value of zero where the timing of infection incidence is dispersed uniformly across the year and of one where all infections occur on the same day of the year.



Appendix Figure 10: Exemplar calculation of the circular mean and variance. Infection incidence time-series (following burn-in) is displayed around the circle by time of year t_{mod} for $r = 0.06, \eta = 0.37$ (all other parameters as in Table 1). We have a mean vector of $(\bar{x}, \bar{y}) = (0.417, -0.549)$, corresponding to an angle of $\theta = 5.37$ and mean day of infection $\bar{d} = 312$. The circular variance is $v = 0.311$.